catalysts

MDPI

Article

Synthesis and Characterization of Zinc Oxide Nanoparticles Using *Acacia caesia* Bark Extract and Its Photocatalytic and Antimicrobial Activities

Jayachandran Ashwini [1,*], Thankamani Ravikumar Aswathy [1], Anil Babu Rahul [2], Gautham M. Thara [2] and Achuthsankar S. Nair [1]

[1] Department of Computational Biology & Bioinformatics, University of Kerala, Thiruvananthapuram 695581, Kerala, India; aswathyravikumartr@gmail.com (T.R.A.); sankar.achuth@gmail.com (A.S.N.)
[2] Department of Biotechnology, Sree Chithra Thirunal College of Engineering, Thiruvananthapuram 695018, Kerala, India; rahulsctbt@gmail.com (A.B.R.); tharagauthamm@gmail.com (G.M.T.)
* Correspondence: ashwinijayachandrans@gmail.com

Abstract: This paper presents the green synthesis and characterization of ZnO nanoparticles and their microbial and photocatalytic application. The green synthesis of ZnO nanoparticles was carried out using Zinc nitrate hexahydrate and the bark extract of *Acacia caesia* (L.) *Willd*. The nanoparticles were synthesized at an optimum temperature of 65 °C followed by calcination at 400 °C. The samples were characterized using UV-visible spectroscopy, SEM, XRD, FTIR and EDX analysis. UV-visible spectroscopy showed a characteristic peak at 338 nm and the bandgap energy was found to be 3 eV which is specific for ZnO. SEM confirmed the presence of ZnO on its nanoscale. EDX gave the elemental details of Zinc constituting to 37.77% and Oxygen comprising 20.77% of its atomic weight. XRD analysis gave the diffractogram indexed at various angles corresponding to ZnO nanoparticles. It also revealed the average crystalline size to be 32.32 nm and the shape was found to be hexagonal. The functional group present in the nanoparticles was characterized using FTIR, which gave a characteristic peak at 485 cm^{-1}. The synthesized nanoparticles exhibited significant photocatalytic (methyl blue under UV irradiation). The presence of nanoparticles induces changes in its kinetics, whose rate constants and correlation coefficients were analyzed during the photocatalytic degradation of the model pollutant Methyl Blue. Studies on antibacterial (*Escherichia coli*, *Staphylococcus aureus*), antifungal (*Aspergillus niger*, *Candida albicans*) and anti-inflammatory (COX assay) properties were also carried out. The nanoparticles were synthesized in an eco-friendly and cost-effective method. The study opens new horizons in the field of water treatment, biosensors and nanotechnology.

Keywords: green synthesis; *Acacia caesia* (L.) *Willd*; eco-friendly; Zinc oxide nanoparticles; photocatalytic; water treatment; antimicrobial

Citation: Ashwini, J.; Aswathy, T.R.; Rahul, A.B.; Thara, G.M.; Nair, A.S. Synthesis and Characterization of Zinc Oxide Nanoparticles Using *Acacia caesia* Bark Extract and Its Photocatalytic and Antimicrobial Activities. *Catalysts* **2021**, *11*, 1507. https://doi.org/10.3390/catal11121507

Academic Editors: Ludovico Valli, Rosanna Pagano and Zois Syrgiannis

Received: 30 October 2021
Accepted: 6 December 2021
Published: 10 December 2021

1. Introduction

Nanotechnology has always been a point of interest for scientists all over, owing to their peculiar properties and potential application, thereby an active research topic [1,2]. They are of major innovative importance in various domains such as nanomedicine [3,4] and antimicrobial [5,6]. These engineered marvels have found promising applications in the construction of biosensors [7,8]. Nanomaterials have not only high specific surface area but also have a high surface area to volume ratio, which increases with a decrease in size, distribution and morphology of the particles [9,10]. Furthermore, these superior physical properties make the nanoparticles more reactive [11].

Chemical synthesis of nanoparticles often poses a number of subsequent problems, such as the presence of toxic chemical species which may get absorbed on the surface of the nanoparticles as a result of the synthesis process, which in turn makes them unsuitable

for any biomedical processes [12–14]. In addition, the conventional chemical methods are often too expensive to carry out due to the need for expensive chemical reducing agents [15,16]. Hence there necessitates a need for the synthesis of less toxic, more eco-friendly nanoparticles synthesis method, which is achieved by green synthesis [17–19]. Green synthesis methods utilize bacteria, fungi, macro/microalgae and plant parts for the synthesis [20–23]. Among green synthesis techniques, synthesis using plant extracts offers a more significant promise owing to their ease of availability, less biohazardous properties and negates the involvement of cell culturing practices [24–26]. Plant parts like root, bark, fruit, flower, leaf etc. have been used in the past for the synthesis of nanoparticles [27–31]. For the present study for the synthesis of nanoparticles, bark extract has been used.

Metal oxide nanoparticles offer an area of interest owing to their distinctive optical, magnetic, catalytic and electrical properties [32]. Moreover, they possess unique characteristics such as surface plasmon resonance hence are being extensively used in the field of optical imaging [33]. Amongst the various metal oxides, Zinc oxide is found to be a potential candidate in the field of biomedical, especially for antimicrobial, anti-cancer, anti-diabetes, anti-inflammatory, cell imaging, and biosensing applications [34–37]. In addition, zinc oxide nanoparticles form the ideal candidates for applications involving biological materials owing to their easy fabrication, non-toxicity, biocompatibility and biosafety [11,38,39].

This paper presents the synthesis of ZnO nanoparticles using the bark extract of the plant *Acacia caesia* (L.) *Willd*. It is an Indian medicinal plant with a rich phytochemical profile [40]. The bark of the woody shrub has been shown to possess numerous therapeutic properties such as antimicrobial activities, insecticidal and wound healing [41,42]. *Acacia caesia* (L.) *Willd.* has also been shown to exhibit antioxidant activity comparable to ascorbic acid [43]. Previously, *Acacia caesia* (L.) *Willd.* leaf extract has shown great promise in silver nanoparticle fabrication, which exhibited considerable activity against the hatching and growth of mosquito vectors [40]. This is the first time that the bark extract of *Acacia caesia* (L.) *Willd.* has been used for the formulation of Zinc oxide nanoparticles. Scheme 1. shows the mechanism of nanoparticle synthesis. From the figure, Methoxyeugenol complex formation is an assumption based on the structure of the compound and, owing to the class of compound it belongs to, based on previous literature [44]. Phenolic compounds have been reported to have a high affinity to form complexes with metals as they are potent metal chelators. In particular, eugenol has been studied and found to possess chelating potential with metals. Methoxy group has also been reported to serve an auxillary for complex formation with metals and have been reported to show an increasing antioxidant property. The flavanoid moieties are known to initiate capping of Zn^{2+} ions while phenolic compounds have been reported to stabilize ZnO nanoparticles after nucleation and also aid in the formation of multi-chelating bonds and thereby result in the formation of different sized nanoparticles.

ZnO nanoparticles also have great photocatalytic activity among all the inorganic photocatalytic materials because of their advanced oxidation property. They are widely used for the removal of pollutants like dyes, toxins and pigments from the environment [45–47]. The mechanism involved in the degradation of the pollutant is illustrated in Scheme 2. When irradiated with UV light, the electrons from the valence band get quickly excited and jump to the conduction band. ZnO is an n-type semiconductor with a wide bandgap of 3.37 eV [48] and a large exciton binding energy of 60 meV [49]. This results in the generation of electron-hole pairs as there will be vacant sites in the valence band. Thus, the valence band is accumulated with holes and the conduction band with electrons. These hole in the valence band, upon reaction with water molecules forms hydroxyl groups which when reacts with the dye produce the degradation products along with carbondioxide and water. The degradation can also happen due to the reaction between the oxygen atoms with the electrons in the conduction band reducing the oxygen to O_2^-.

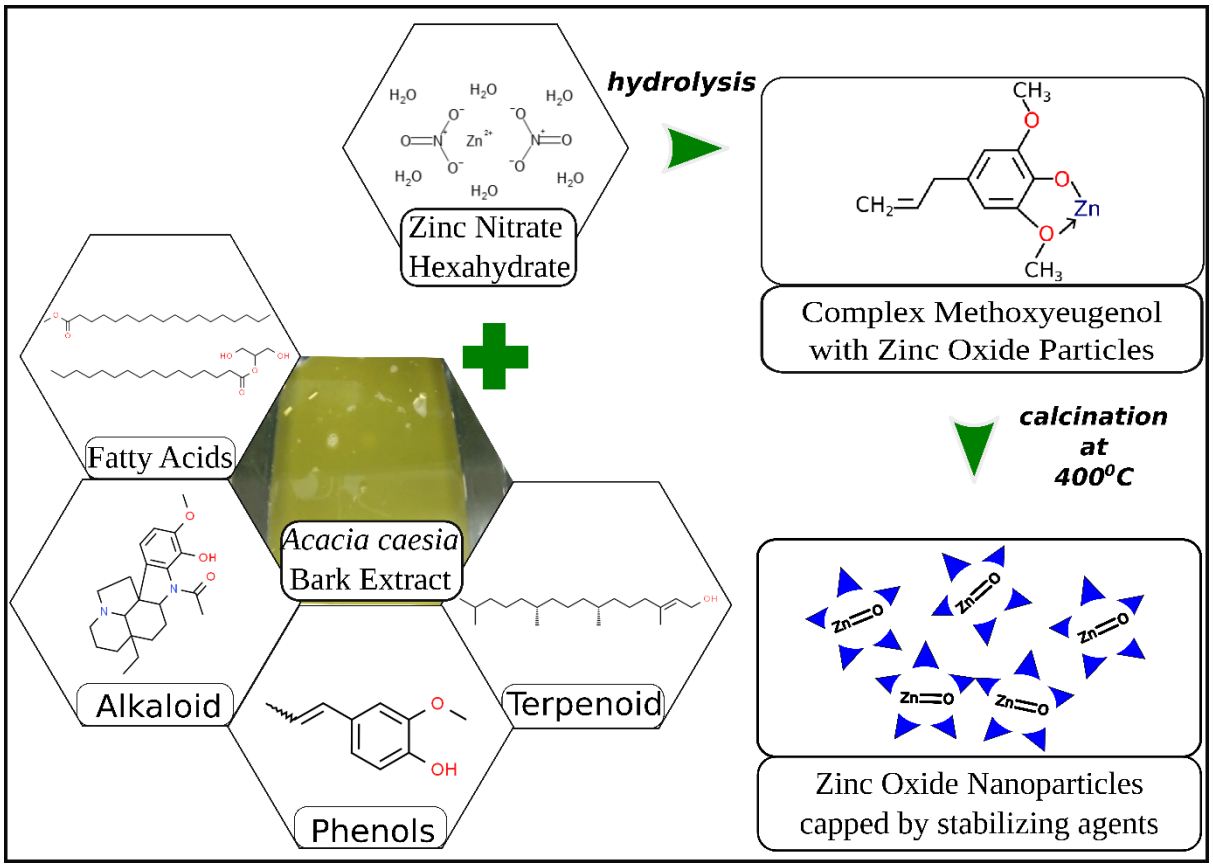

Scheme 1. Probable mechanism of Zinc oxide nanoparticle formation from the bark extract of *Acacia caesia* (L.) *Willd.*.

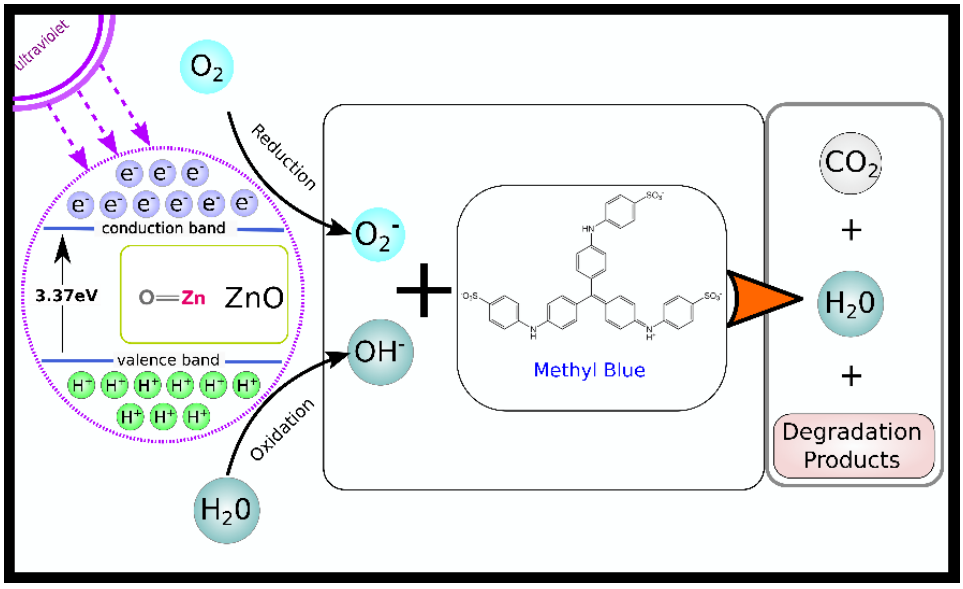

Scheme 2. Mechanism of photocatalytic dye degradation using Zinc oxide nanoparticles.

Recent studies have reported that the use of nanomaterials resulted in high-performance waste water treatment [50–52]. Various environmental friendly methods like the embedded ZnO nanoparticles in a surface layer of clay used as a matrix has been reported in the past for the adsorption and photocatalytic degradation of pollutants in wastewater [53]. Wang et al. investigated and synthesized a novel clay nano-based catalyst of ZnO/TiO_2/rectorite for photodegradation and adsorption of methylene blue from the aqueous phase [54]. Several studies also revealed that the same experiment using different dyes in varying

conditions showed the degradation of the photocatalytic activity of the nanocomposites in the removal of the dyes [55–57]. For the present study, a model pollutant like methyl blue was considered for the analysis whose photocatalytic activity was measured in terms of percentage degradation of the dye.

Another application the study put forward is in the antimicrobial activity of the synthesized nanoparticles. The use of ZnO nanoparticles may be a promising alternative to antibiotics and it can act against a diversity of microorganisms, such as *S. aureus,* [58] *E. coli* [59] and *C. albicans* [60,61]. Several studies revealed that the antibacterial and antifungal activity of ZnO nanoparticles is based on the formation of reactive oxygen species (ROS) such as superoxide anion, hydroxyl radicals, and hydrogen peroxide production. These ROS interacts with the cell causing oxidative stress and subsequently cell damages, thus resulting in antimicrobial activity [62,63]. Another mechanism is the release of Zn^{2+} ions, which would cause bacterial cell membrane disintegration, membrane protein damage and death of bacterial cells [64,65]. The other possible mechanism is the nanoparticles entering the bacteria cell membrane via electrostatic forces and the loss of cellular integrity resulting in cell death [66]. Moreover, ZnO nanoparticles have anti-inflammatory and anti-cancer properties and several studies reported that it is an excellent anti-inflammatory agent by dose-dependently suppressing both mRNA and protein expressions of iNOS, COX-2, IL-1β, IL-6 and TNF-α [67].

The present paper discusses the Green synthesis of ZnO nanoparticles from the herbal medicinal Plant *Acacia caesia* (L.) *Willd.* followed by characterization, photocatalytic degradation activity of dye Methylene Blue, antimicrobial and anti-inflammatory properties.

2. Results and Discussions

2.1. XRD Analysis

The diffractogram was analyzed to understand the crystalline nature of the synthesized nanoparticles. The X-ray diffraction peaks of green synthesized ZnO nanoparticles using *Acacia caesia* (L.) *Willd.* at 2θ obtained are at 31.61°, 34.28°, 36.10°, 47.4°, 56.45°, 62.72°, 67.8°, 68.93°. The peaks were matched with the ICDD card number 01-089-0511, and the shape of the crystal was found to be hexagonal in nature. From the ICDD card details, the crystalline shape was identified from the space group ($P6_3mc$) and space group number (No.186) and the lattice parameter a (equal to b) was found to be 3.2490 Å and c was found to be 5.2052 Å which matches with the values previously reported [68]. In the XRD analysis of nanoparticles, crystal planes were detected, as shown in Figure 1 which correspond to the lattice planes (hkl) indexed as (100), (002), (101), (102), (110), (103), (112), and (201) respectively as shown in Table 1. A reference image of ZnO nanoparticle formed using the chemical synthesis method is shown in the inset [69] which is in accordance with the XRD reported in this paper. Apart from the major peaks, some minor peaks can also be seen at 23.5, 28.1, 29.2, 40.3, 41.03, 67.8, 72.4 and 76.8 which is attributed to the formation of certain compounds due to the presence of the elements Sodium and Carbon as detailed in Section 2.3.

Table 1. Crystal planes and particle size details from the XRD analysis of ZnO nanoparticles synthesized using *Acacia caesia* (L.) *Willd.* at different diffraction angles.

Sl. No.	2Θ	FWHM (β)	Miller Indices	Particle Size D (nm)
1	31.61	0.0039	(100)	36.48
2	34.28	0.0039	(002)	36.74
3	36.10	0.0043	(101)	33.56
4	47.40	0.0047	(102)	31.94
5	56.45	0.0055	(110)	28.46
6	62.72	0.0063	(103)	25.69
7	67.80	0.0055	(112)	30.21
8	68.93	0.0047	(201)	35.48

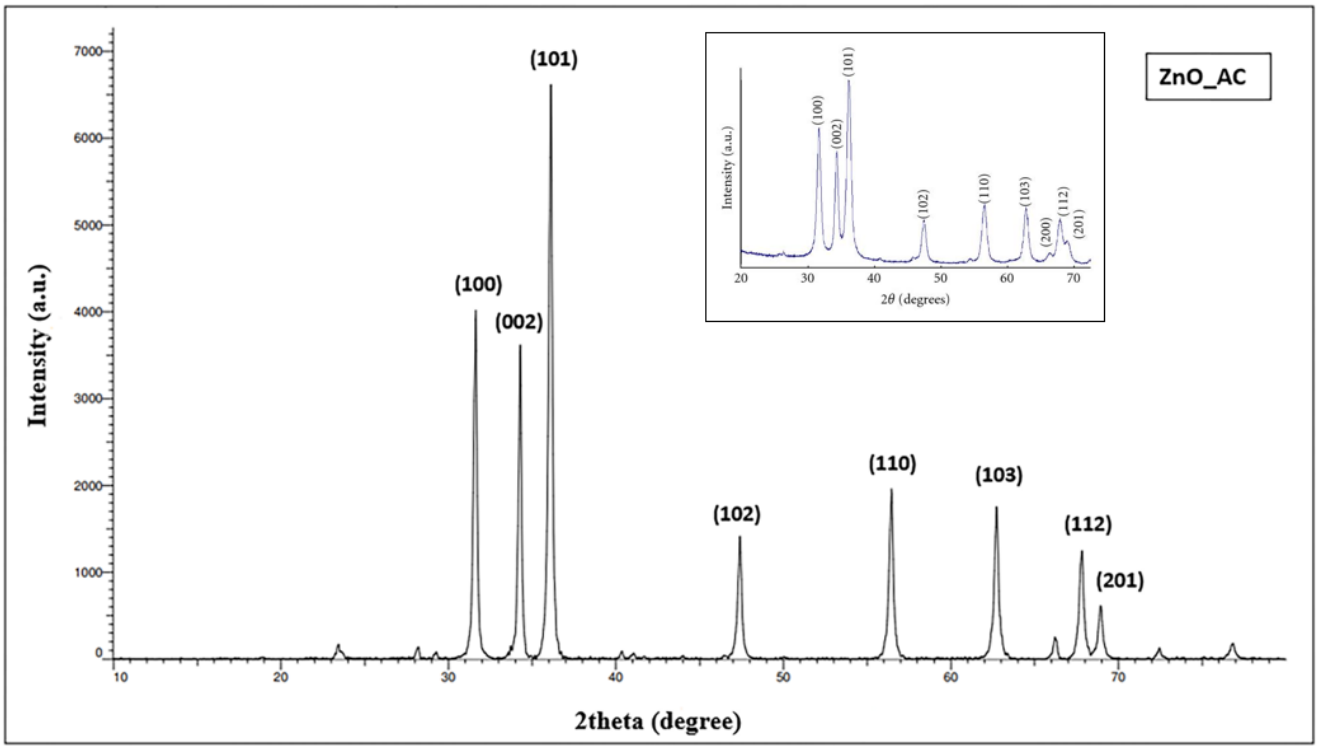

Figure 1. X-ray diffractogram of synthesized Zinc oxide nanoparticles along with a reference diffractogram.

The synthesized nanoparticle's crystalline size varies from as small as 25.69 nm to as high as 36.48 nm. The average crystalline size of the particles was found to be 32.32 nm.

2.2. SEM Analysis

The Scanning Electron Microscopic images were taken to confirm the presence of nanoparticles. Figure 2 shows SEM taken at different magnifications—10,000×, 25,000×, 50,000× and 100,000×. The particles were in an agglomerated form. From the Figure 2. A depicts a more spherical shape. On a closer note, as seen in B, fibre shaped particles were more evident. These fibrous formed hexagonal shaped particles when figures of various magnifications were analyzed. SEM revealed the particle to be in its nano form. The partially agglomerated state could be due to the fact that no hard-acting chemical filtration methods were employed in green synthesis. Another factor that promotes aggregation can be the smaller size of the nanoparticles.

2.3. EDX

The EDX graph provides the elemental details of the synthesized ZnO nanoparticles as shown in Figure 3. The weighted percentage of Zinc and Oxygen was 37.77% and 20.77%, respectively. Apart from Zinc and Oxygen, there were traces of other compounds like Carbon, Sodium etc. The presence of other major peaks might be as a result of X-ray emissions breaking down capping agents such as polysaccharides, proteins, amino acids and sugars [70,71]. When kept at room temperature for long, the synthesized particles will react with moisture and carbon dioxide to form other compounds. That is why a trace of carbon is found at 0.277 eV.

The table in Figure 3 gives the atomic and the weight percentage of the elements in the nanoparticles. X-ray.

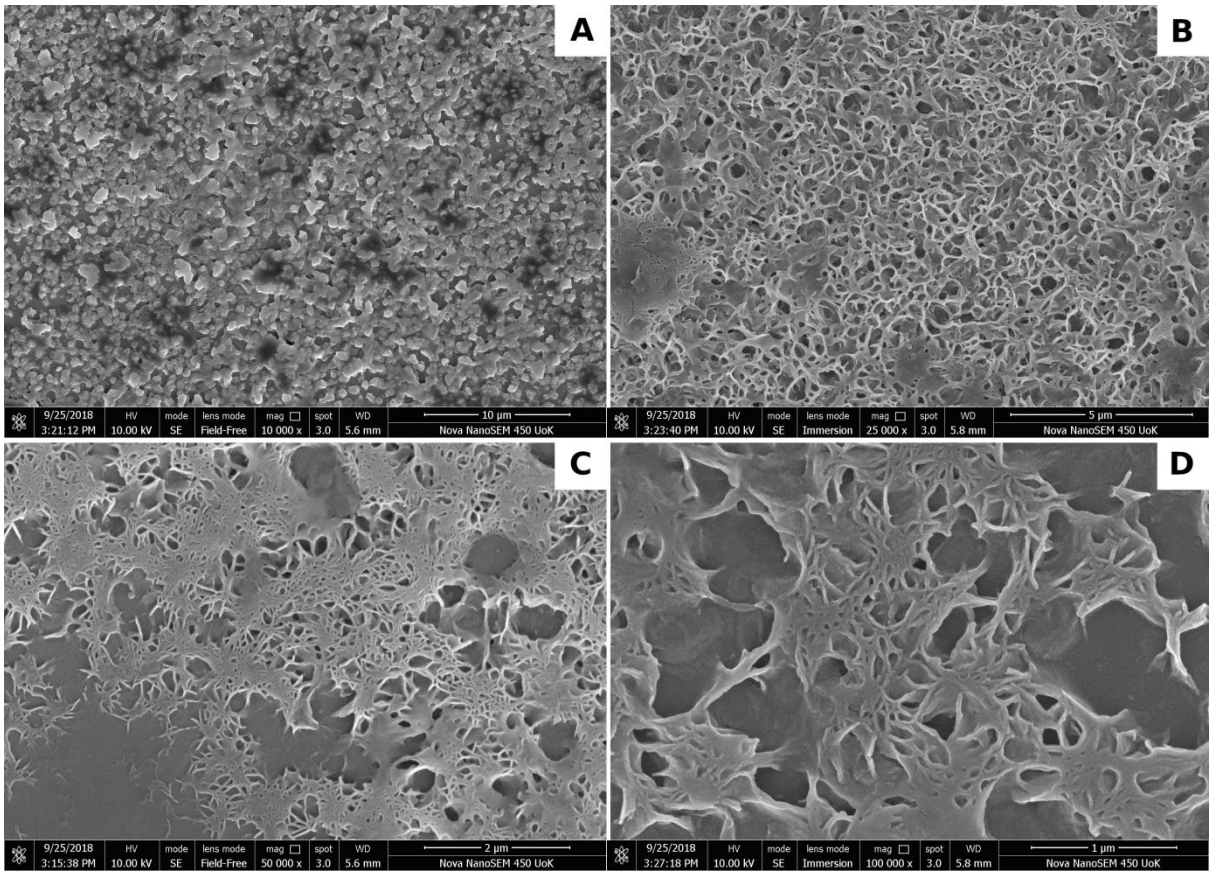

Figure 2. FESEM images of ZnO nanoparticles at various magnifications (**A**) 10,000× (**B**) 25,000× (**C**) 50,000× (**D**) 100,000×.

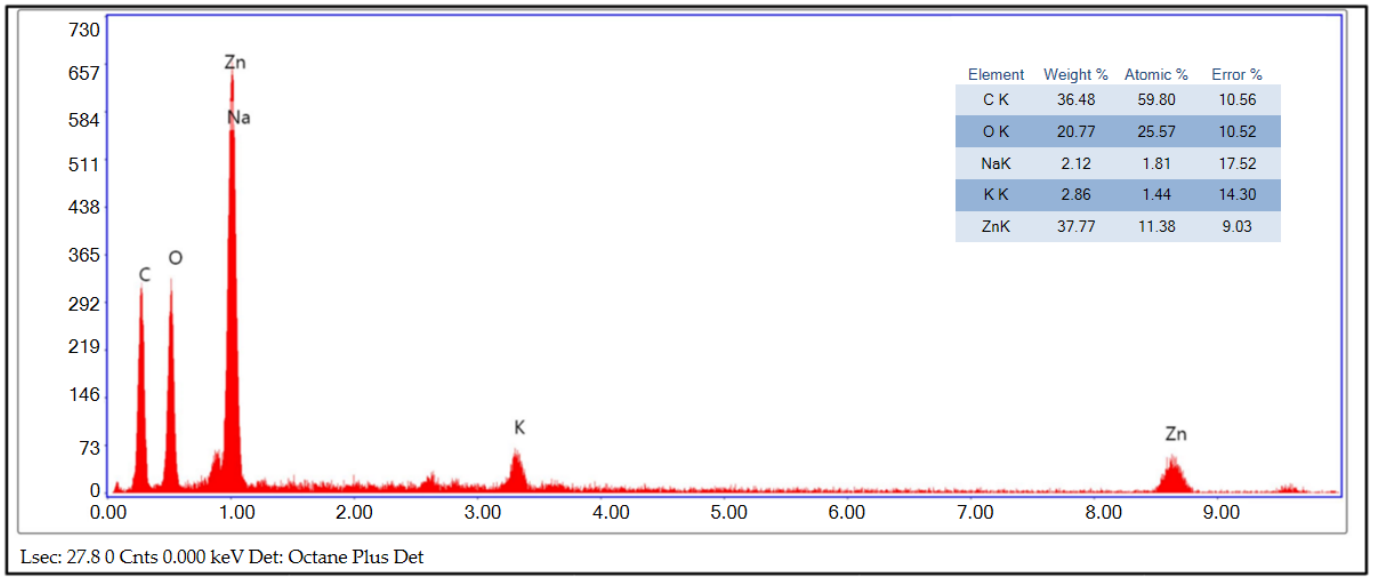

Figure 3. EDX spectrum of synthesized Zinc oxide nanoparticles.

2.4. UV-Visible Spectroscopy

The preliminary confirmation of the presence of zinc oxide was carried out by UV-Visible spectral analysis. The suspension concentration was 0.2 mg/mL. The sample exhibited a peak absorption at 338 nm as shown in Figure 4 is in accordance with the spectral range of ZnO nanoparticles, between 300–500 nm [17,72]. The bandgap energy

was found to be 3 eV. This was calculated using Tauc's plot obtained from the values of the UV spectrum. The intercept of Tauc's plot directly gives the measure of the energy gap [73].

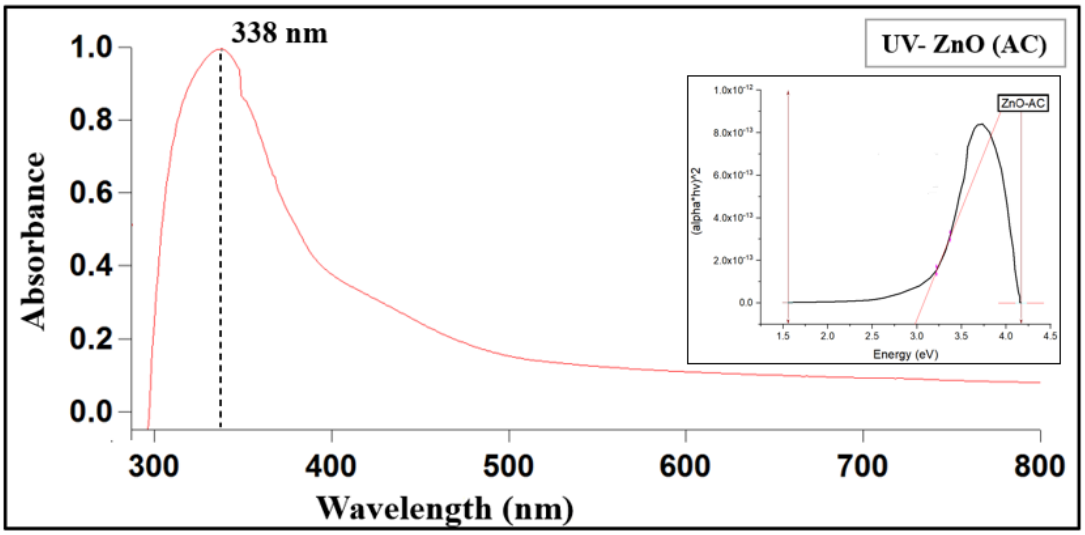

Figure 4. UV-Vis spectrum of Zinc oxide nanoparticles with Tauc's plot in the inset showing energy band gap intercept at 3 eV.

When zinc nitrate hexahydrate is added to the aqueous extract of the *Acacia caesia* bark and heated, the formation of yellow colour serves as a visual confirmation on the formation of compounds of zinc nanoparticle [16,74]. This may also be due to the formation of Zinc oxide from Zinc nitrate hexahydrate using the secondary metabolites present in the plant extract as reported in the past. The change of colour to yellow may be attributed to oxygen deficiencies as Zinc oxide nanoparticles are heated

$$ZnO = Zn^{2+} + \frac{1}{2} O_2 + 2e^-$$

This results in the movement of excess zinc ions into the interstitial space followed by electrons into the adjacent interstitial spaces and formula becomes $Zn_{1+x}O$. As the anionic oxygen moves to bind with the cationic Zn^{2+} species, electrons will fill the anionic vacancies thereby forming F-centres which imparts the yellow color [75].

2.5. FTIR

The FTIR spectral profile details about the functional groups present in the synthesized ZnO nanoparticles. It also portrays that the formation of ZnO nanoparticles is due to the interaction of the phenolic compounds, alkenes, amines, terpenoids, and flavonoids. FTIR spectra of the synthesized ZnO nanoparticles using *Acacia caesia* (L.) *Willd.* was analyzed in the range 400 to 4000 cm^{-1}. Conversion of Zinc ions to Zinc oxide was observed as bands which resulted in the formation of Zinc oxide nanoparticles. Each of the bands corresponds to various stretching and bending modes. From Figure 5, the band corresponding to hydroxyl group stretching is observed at 3258 cm^{-1}. This is due to the interaction of OH group in water by H bond which is observed as a stretching mode. The bending at 1630 cm^{-1} is attributed to the H-O-H bonding due to the water molecules adsorbed on the surface [76]. This hydroxyl stretching with HOH bending together accounts to the strength of the water molecules to the anion [77]. Moreover, this bending has contributed to the peak intensity which can be observed in 1312 cm^{-1}. The region at 1053 cm^{-1} corresponds to –C–O–C stretching bonds whereas the spectra with wavenumber below 500 cm^{-1} correspond to the presence of metal oxides, and the stretching at 485 cm^{-1} confirms the presence of ZnO [78]. It can also be noted that there is an increase in the peak of the functional group amine at 1312 cm^{-1} which is due to the presence of carbon

as briefed in Section 3.2. However, the XRD spectra give clear information regarding the compound ZnO even though traces of other compounds can be found.

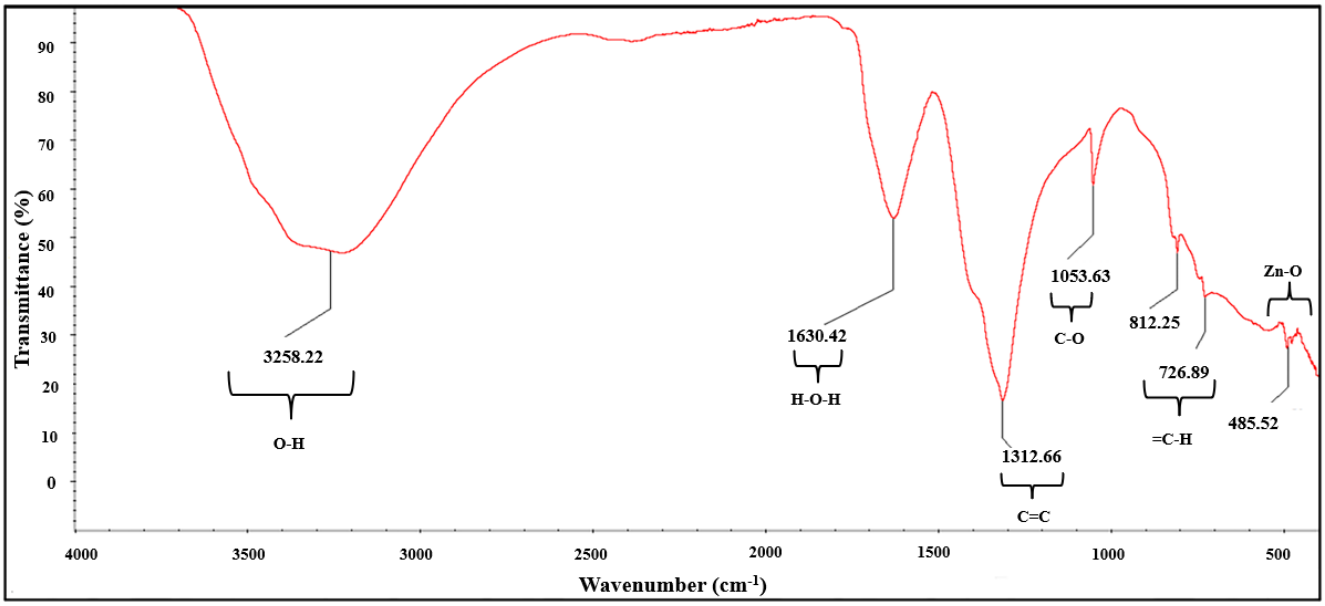

Figure 5. FTIR spectrum of synthesized Zinc oxide nanoparticles.

2.6. Photocatalytic Activity

The absorption spectra were taken for the model pollutant Methyl blue at 0.06 mg/mL and 0.03 mg/mL for two different concentration of ZnO (0.2 mg/mL and 0.1 mg/mL). The spectrum showed a maximum wavelength, λ_{max} at 601 nm for both the concentration of ZnO nanoparticles which is specific for MB [79]. During the experimentation, the ZnO nanoparticles were kept in the dark for 10 min for observation and the dye did not show any degradation. While the absorption drastically changed over a period of 40 min when ZnO was added to the same stock solution and exposed to UV light radiation, as shown in Figure 6a. For a higher concentration of ZnO, the absorption at 0 min was higher than the sample with a lower ZnO concentration. This is due to the fact that more the concentration of ZnO nanoparticles, more will be the molecules that interacts with light waves leading to higher absorption. At the end of 40 min for both the samples, the absorption has reduced and are comparable.

The degradation percentage showed 92% of the dye had degraded for a higher concentration of ZnO nanoparticles (0.2 mg/mL), whereas the dye degradation was only 83% at the end of 40 min for the lower concentration of ZnO (0.1 mg/mL) as shown in Figure 6b. The present paper reports 50% dye degradation within 8 min, which is twice as fast when compared to previously reported paper using the same precursor for the green synthesis of ZnO nanoparticles [80]. For MB dye at 0.03 mg/mL, when ZnO with a higher concentration (0.2 mg/mL) was added, the absorption reduced in an exponential manner as shown in Figure 7a. It may also be noted that in the case ofMB added with ZnO nanoparticle of lower concentration (0.1 mg/mL), the absorption decreases almost in a linear manner. Figure 7b shows the degradation percentage for ZnO with higher concentration. It shows a degradation of 85% and the MB added with ZnO nanoparticle of lower concentration (0.2 mg/mL) added, the degradation percentage is as low as 61%.

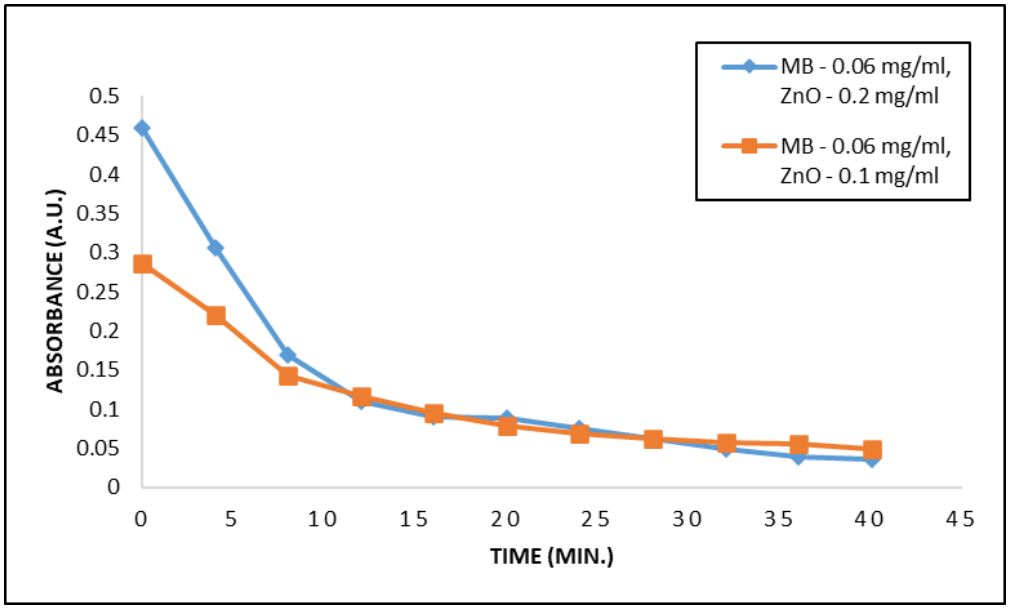

(**a**)

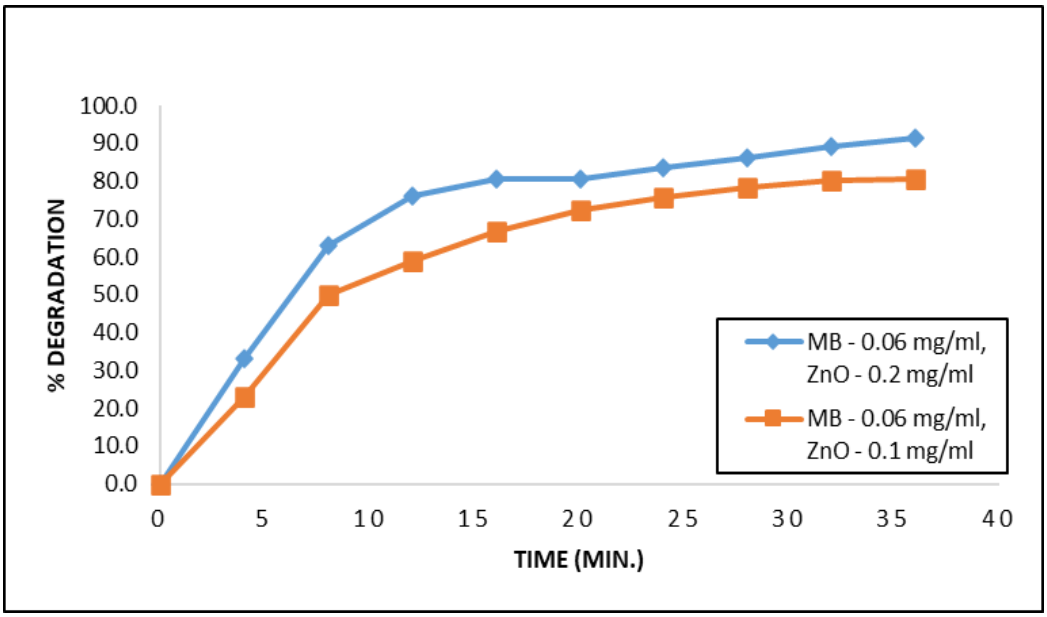

(**b**)

Figure 6. Graph showing the photocatalytic degradation of the model pollutant MB at 0.06 mg/mL with varying ZnO nanoparticle concentration (**a**) Absorption (**b**) %degradation.

Rate constant has been calculated for all the four cases (A to D) using Langmuir Hinshelwood equation. The rate constant ideally should follow the first order reaction which is linear as shown in Figure 8. The slope, intercept and the R^2 values are shown in Table 2. Figure shows the kinetics of MB at two different concentrations (0.06 mg/mL and 0.03 mg/mL) with ZnO nanoparticles added reaction at two different concentrations 0.2 mg/mL and 0.1 mg/mL. The slope of the equation directly gives the rate constant. The rate constant for cases A, B, C and D are 3.16×10^{-4}/s, 1.75×10^{-4}/s, 2.19×10^{-4}/s and 1.13×10^{-4}/s respectively. These values of the rate constant are in accordance with the previously reported work [81]. When compared to case D, the rate constant of A is three times as reported in a similar study earlier [82].

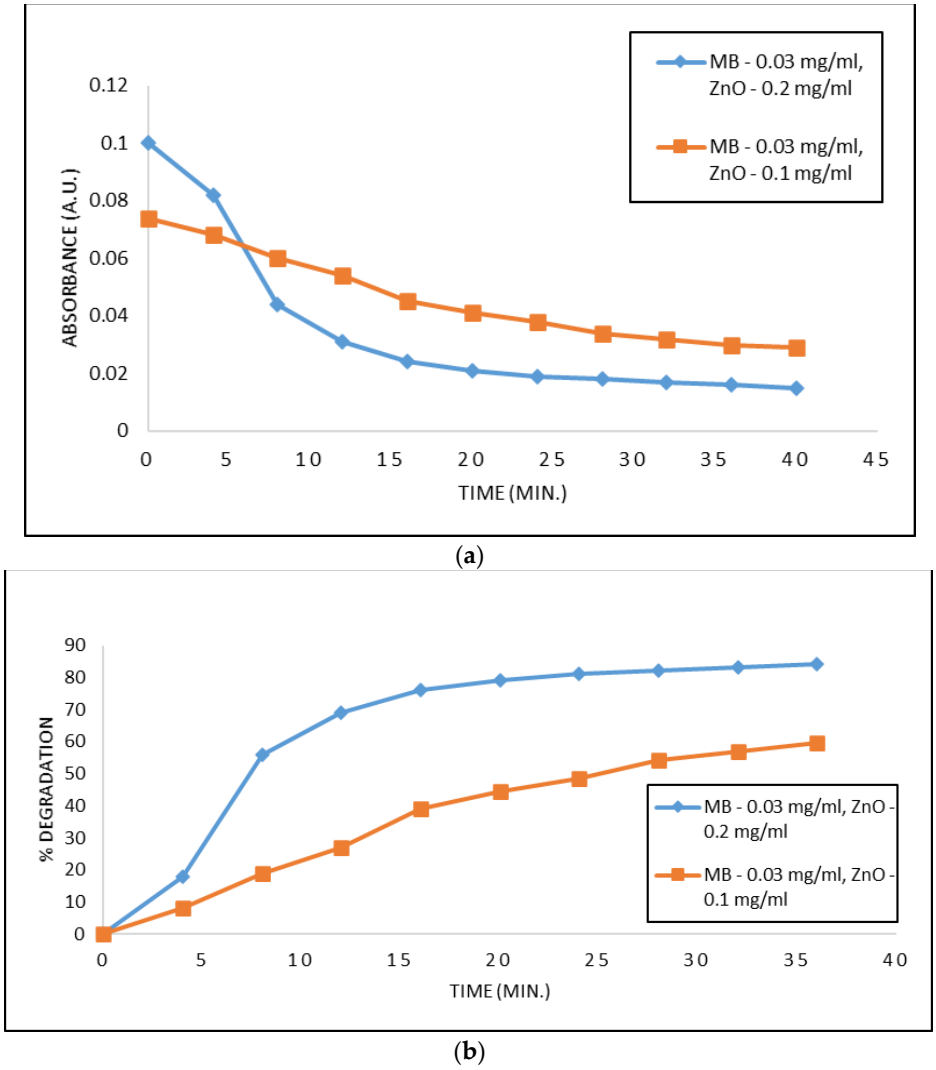

Figure 7. Graph showing the photocatalytic degradation of the model pollutant MB at 0.03 mg/mL with varying ZnO nanoparticle concentration (**a**) Absorption (**b**) %degradation.

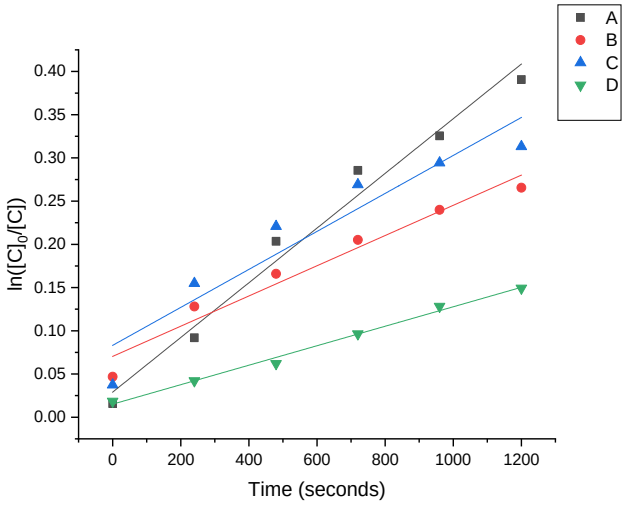

Figure 8. Graph illustrating the kinetics of the photocatalytic activity with varying concentration of dye and nanoparticles (**A**) MB—0.06 mg/mL, ZnO—0.2 mg/mL (**B**) MB—0.06 mg/mL, ZnO—0.1 mg/mL (**C**) MB—0.03 mg/mL, ZnO—0.2 mg/mL (**D**) MB—0.03 mg/mL, ZnO—0.1 mg/mL.

Table 2. Values of concentration of MB, ZnO, first order rate constants and correlation coefficients for the photocatalytic degradation of MB.

Notation	Concentration of MB (mg/mL)	Concentration of ZnO (mg/mL)	Rate Constant	Intercept	R^2
A	0.06	0.2	3.16×10^{-4}/s	0.029	0.98
B	0.06	0.1	1.75×10^{-4}/s	0.071	0.96
C	0.03	0.2	2.19×10^{-4}/s	0.083	0.90
D	0.03	0.1	1.13×10^{-4}/s	0.015	0.99

2.7. Anti-Inflammatory Activity of ZnO Nanoparticles

The inhibition of cycloxygenase enzyme by ZnO nanoparticles at different concentrations (25, 50, 100 µg/mL) were analyzed and compared against Acetylsalicylic acid, used as the reference compound. The results are summarized in Figure 9. The percentage of inhibition by the ZnO nanoparticles and Acetylsalicylic acid were 23.41% and 34.51%, respectively, at a concentration of 25 µg/mL each. At a treatment level of 50 µg/mL the percent inhibition by the lead compound ZnO nanoparticles was 34.24% and that of Acetylsalicylic acid was 51.80%. Among the three different concentrations, the concentration of 100 µg/mL ZnO nanoparticles showed higher percentage of inhibition (64.81%).

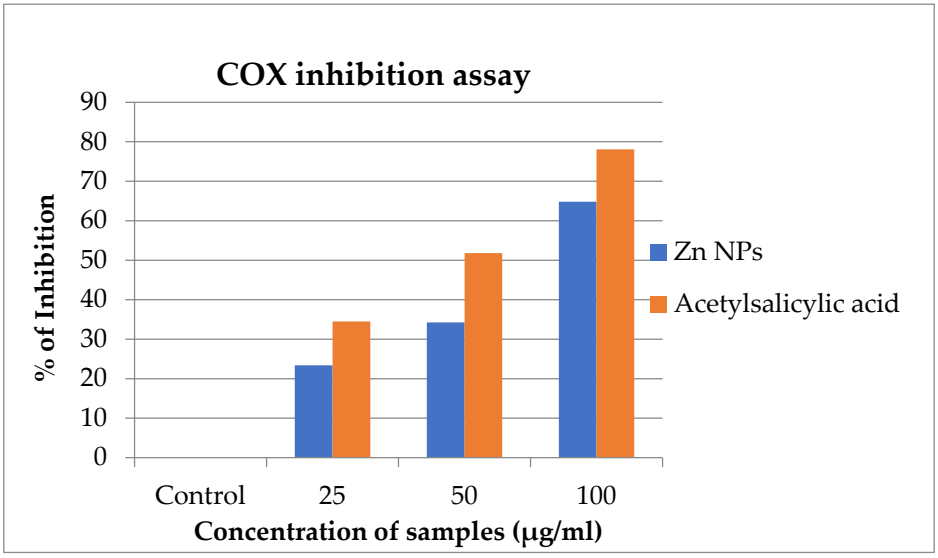

Figure 9. Percentage inhibition of COX enzyme.

The results reveal that at a higher concentration of Zn nanoparticles, high percentage of inhibition like the reference drug Acetylsalicylic acid is exhibited. The study thus shows that green synthesized Zn nanoparticles possess good anti-inflammatory activity. Nagajyothi et al. observed that green synthesized ZnO nanoparticles using the root extract of *P. tenuifolia* have anti-inflammatory activities using LPS-stimulated RAW 264.7 macrophages [67]. Moreover, previous studies have reported that the biomediated synthesis of ZnO nanoparticles using *Lantana Camara* flower extract has high anti-inflammatory properties [83]. Furthermore, studies also investigated that the small-sized ZnO nanoparticles have significant effects on reducing skin inflammation [84] using in different-sized ZnO nanoparticles penetrate injured skin in the mouse model.

2.8. Antimicrobial Activity of ZnO Nanoparticles

2.8.1. Antibacterial Activity of ZnO Nanoparticles

The antibacterial activity of ZnO nanoparticles was examined against Gram-negative (*Escherichia coli* ATCC 25922) and Gram-positive (*Staphylococcus aureus* ATCC 25923) bacterial strains by using the disc diffusion method. Different concentrations (250 µg, 500 µg and 1000 µg) of the samples were prepared and used. The result is shown in Table 3 and

Figure 10. The green synthesized ZnO nanoparticles using *Acacia caesia* (L.) *Willd.* bark extract exhibited strong antibacterial activity against both Gram-negative (*E. coli*) and Gram-positive (*S. aureus*) bacteria strains. The 1000 µg/mL concentration of ZnO nanoparticles showed a maximum inhibition zone in both strains. Various studies reported that green synthesized ZnO nanoparticles show high bactericidal activity in both strains [85–87].

Table 3. Antibacterial activity of ZnO nanoparticles.

ZnO Nanoparticle Concentration (µg)	Zone of Inhibition (mm) (Diameter)	
	E. coli	*S. aureus*
250	15	11
500	17	12
1000	18	13
Streptomycin (100 µg)	25	25

(**a**) (**b**)

Figure 10. Antibacterial activity of ZnO nanoparticles against (**a**) *E. coli* and (**b**) *S. aureus*.

In the present study, it was found that the green synthesized ZnO nanoparticles showed a more significant inhibitory effect on the Gram-negative bacteria (*E. coli)* in contrast to a lower activity on Gram-positive bacteria (*S. aureus*). However, previous studies reported that green synthesized zinc oxide nanoparticles have great antibacterial potential on Gram-positive than Gram-negative bacteria [88]. The Gram-negative has a lower thickness, when compared to a much larger thickness in Gram-positive bacteria, of peptidoglycan layer which plays a primary role in maintaining cell integrity. The cell walls of Gram-negative bacteria are more complex in layout than the Gram-positive ones acting as a diffusion barrier and making them less susceptible to the antibacterial agents [86]. This observed difference could be attributed to the plant extract were used structural differences between Gram-positive and Gram-negative bacteria.

The present study depicted that the zone of inhibition by the *E. coli* and *S. aureus* were 15 mm and 11 mm, respectively, at a concentration of 250 µg/mL each. At the concentration of ZnO NPs 500 µg/mL the zone of inhibition by *E. coli* was 17 mm and *S. aureus* was 12 mm. Gram-negative strain *E. coli* showed higher inhibition (18 mm) at a concentration of 1000 µg/mL in comparison with the Gram-positive strain *S. aureus* (13 mm). The positive control Streptomycin (100 µg) showed a zone of inhibition at 25 mm in both the strains. In the study, it is found that the green synthesized zinc oxide NP showed a more significant inhibitory effect on the *E. Coli* in contrast to a lower activity *S. aureus*. Jiang et al. also

revealed the potential antibacterial mechanisms of ZnO nanoparticles against *E. coli* [59]. The activity of the crude extract of the plant against *E. coli* and *S. aureus*, reported in our previous work [41] showed that the plant extract alone does not show significant activity at low concentrations.

The exact mechanism for the interaction of nanoparticles with bacteria that causes cell disruption is not known, but there have been numerous proposed mechanisms. One mechanism suggests the formation of reactive oxygen species (ROS), which interacts with the cell causing oxidative stress and subsequent cell damage, thus resulting in antibacterial activity [88]. Another mechanism suggests a relationship between the structural relationships of the nanoparticles with the cell. Smaller nanoparticles have a greater surface reactivity and hence could penetrate easier into the cell to release Zn^{2+}. The release of Zn^{2+} from ZnO nanoparticles is known to disrupt cell processes, including active transport, bacteria metabolism, and enzyme activity and thus leading to bacterial cell death [89]. The nanoparticles enter the bacteria cell membrane via electrostatic forces and disrupt the cell is one other possible mechanism. This may distort the membrane plasma structure and damage the bacterial cell integrity resulting in cell death [90].

2.8.2. Antifungal Activity of ZnO Nanoparticles

In the present study the antifungal activity of ZnO nanoparticles was conducted using *Aspergillus niger* (ATCC 16404) and *Candida albicans* (ATCC 10231) fungus through a well-diffusion method. Different concentrations (250 µg, 500 µg and 1000 µg) of the samples were prepared and the results are shown in Table 4 and Figure 11.

Table 4. Antifungal activity of ZnO nanoparticles.

ZnO Nanoparticles Concentration (µg)	Zone of Inhibition (mm) (Diameter)	
	Aspergillus niger	*Candida albicans*
250	11	Nil
500	12	12
1000	14	15
Standard Drug Clotrimazole (100 µg)	29	27

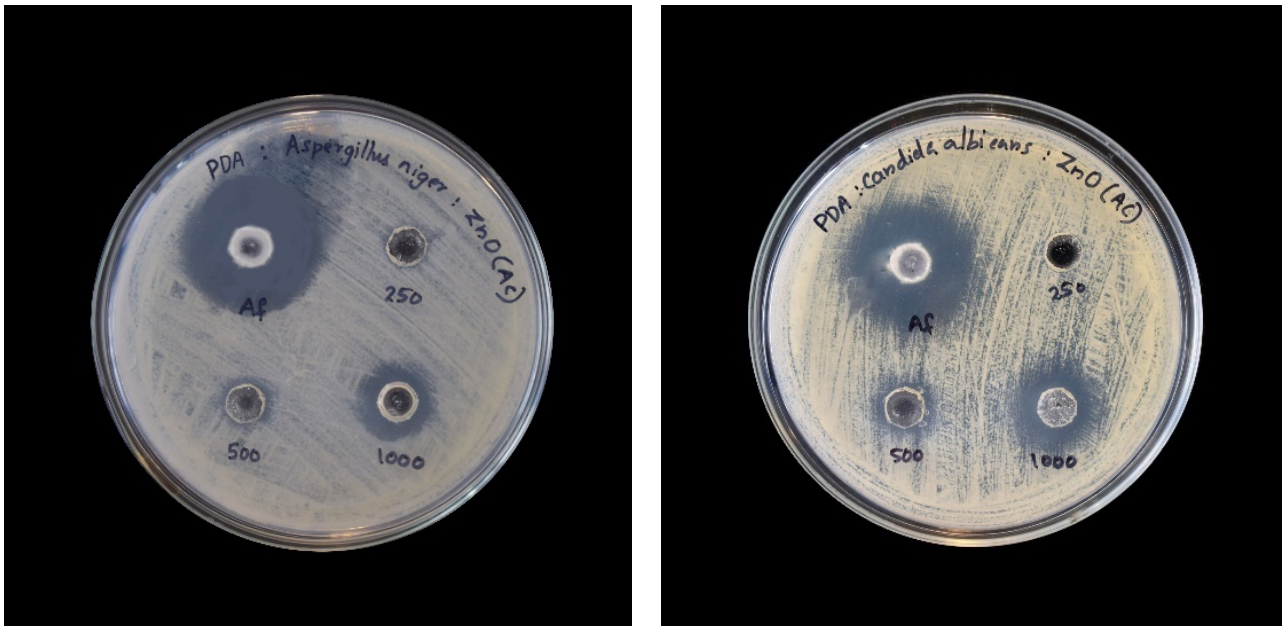

(**a**) (**b**)

Figure 11. Antifungal activity of ZnO nanoparticles against (**a**) *Aspergillus niger* and (**b**) *Candida albicans*.

The value of antibiotic Clotrimazole (100 µg) inhibition zone diameter (positive control) on *A. niger* (ATCC 16404) and *C. albicans* (ATCC 10231) fungus were 29 mm and 27 mm respectively. At the concentration of 250 µg and 500 µg, *A. niger* showed inhibition with a zone diameter of 11 mm and 12 mm respectively. The zone diameter of *C. albicans* was 12 mm at sample concentration of 500 µg. It was found that at concentration of 1000 µg ZnO nanoparticles, the zone of inhibition of *A. niger* and *C. albicans* were 14 mm and 15 mm respectively. The result concluded that the antifungal activity of ZnO nanoparticles is significant, though far less than the standard drug. Previous studies reported that green synthesized ZnO NPs shows high fungicidal activity in both strains [60,91,92]. The antifungal nature exhibited against the organisms could be because of the smaller size of the ZnO nanoparticles. The nanoparticle could penetrate the cell walls and thus inhibit fungal growth due to direct contact with the fungal cell membrane [6,93].

3. Materials and Methods

3.1. Materials for the Synthesis of ZnO Nanoparticles

The bark of *Acacia caesia* (L.) *Willd.* was collected from Pala, Kottayam district, Kerala. A herbarium was deposited at the Department of Botany at the University of Kerala, Kariyavattom in Trivandrum for identification (Voucher Number: KUBH 10097). Zinc nitrate hexahydrate (98% purity), used as the precursor for the synthesis of nanoparticles, was purchased from Merck®.

3.1.1. Preparation of *Acacia caesia* (L.) *Willd* Bark Extract

Freshly procured young green bark of *Acacia caesia* (L.) *Willd.* was washed thoroughly to remove dirt and solid residues from the bark. 25 g of the thoroughly cleaned young bark was cut into small pieces and transferred to a mortar and pestle. 50 mL of distilled water was added to the bark extract to grind the mixture thoroughly to obtain an extremely thick paste. This paste was then pressed to get the aqueous extract of the bark. The solution so obtained was then centrifuged at 2400 rpm for 5 min to remove any persisting debris to get the final liquid aqueous extract which was further taken for the analysis.

3.1.2. Synthesis of Zinc Oxide Nanoparticles

For the synthesis of zinc oxide nanoparticles, the final aqueous extract was boiled in a magnetic stirrer to which 5 mL of 10 mM Zn $(NO_3)_2.6H_2O$ solution was added. The solution developed a slight yellow colour which intensified upon heating for 40 min in a magnetic stirrer at 65 °C. This optimum temperature was chosen after experimenting with temperatures above and below the working temperature. When used 60 °C for the analysis, the yellow colour, which denotes the formation of Zinc complexes with phenolic ligands, was not evident. When a higher temperature of 70 °C was used, it resulted in the formation of ashes. Hence 65 °C was considered as the optimum temperature for the study. Conversion from Zinc nitrate to Zinc complexes takes place during this heating process which is indicated by the formation of a yellow coloured solution. This solution is then subjected to drying by heating the obtained nanoparticle solution at 65 °C overnight to get a thick paste. The paste so obtained was then wholly dried through a process of calcination at 400 °C for 2 h. Calcination is a temperature-dependent process that reduces compounds in their impurity free and powdered form. Calcination also improves the crystalline nature of the nanoparticle and has an effect on the size and shape of the crystal formed [94,95]. This powder is then collected and packed separately for further analysis [96].

3.2. Characterization of Zinc Oxide Nanoparticles

3.2.1. X-ray Diffractogram

X-ray Diffractometer (Bruker AXS D8 Advance) with Cu K-α radiation of wavelength 1.5402 Å was used for analyzing the crystal planes, the shape of nanoparticles and crystalline size determination.

The debye-Scherrer formula was used to calculate the crystalline size of the particles.

$$D = \frac{k\lambda}{\beta \cos\theta} Å \quad (1)$$

where average crystalline particle size is denoted by D, k is the shape factor (0.9), λ corresponds to the wavelength (1.5406 Å) of the X-rays used for diffraction, β corresponds to the full width at half maximum of a peak and θ is Bragg's diffraction angle.

3.2.2. Scanning Electron Microscopy

Sample coated surfaces were analyzed using Nova NanoSEM 450 analyzer. The samples were mixed with acetone and were dried before recording SEM. Multiple SEM images were obtained at accelerating voltages of 5 kV and 10 kV at varying magnifications of 100,000×, 50,000×, 25,000×, 10,000×, at scales of 1 µm, 2 µm, 3 µm, 5 µm and at working distances of 5.8 mm and 5.6 mm.

3.2.3. Energy Dispersive Spectrometry

For the elemental study of the synthesized nanoparticle, Energy dispersive spectrometer—Nova NanoSEM 450 analyzer was used. It gave the atomic weight and elemental composition in terms of energy released due to the bombardment of X-rays.

3.2.4. UV-VISIBLE Spectrophotometry

UV-Vis spectrometric studies were carried out to confirm the presence of nanoparticles. The powdered ZnO NPs were re-suspended in deionized water and UV-Vis spectra was recorded in Cary 100 UV-Vis spectrophotometer G9821A from Agilent Technologies. The spectra were recorded between 300–800 nm wavelength and the solution was sonicated prior to characterization for even distribution. The energy gap value of the absorption spectra was calculated utilizing the Tauc's equation given by

$$(\alpha h\upsilon)^n = A(h\upsilon - E_g) \quad (2)$$

where α is the absorption coefficient, hυ is the photon energy, E_g is the energy bandgap, A is the proportionality constant and n is 2 for direct band transitions [97].

3.2.5. Fourier Transform Infrared Spectroscopy

ThermoFisher-Scientific Nicolet iS50 was used to obtain the FTIR spectrum in order to characterize the functional bonds present in the synthesized nanoparticles. Attenuated total reflectance FTIR was used and pure pellets were considered. 0.5 mg of the sample was taken for the analysis and those samples which are not in a fine powder form should be ground well in order to avoid scattering losses while taking FTIR reading.

3.2.6. Photocatalytic Activity

To investigate the photocatalytic activity of ZnO nanoparticles, an aqueous solution of the dye-ethyl Blue was considered as the model pollutant. Methyl blue (0.03 mg/mL, 0.06 mg/mL) and ZnO (0.1 mg/mL, 0.2 mg/mL) nanoparticles at varying concentrations were taken to evaluate the percentage degradation of the pollutant. To attain adsorption equilibrium, the sample was magnetically stirred before exposing it to radiation. The mixtures were then irradiated under the influence of UV light to assess the activity at regular time intervals (4, 8, 12, 16, 20, 24, 28, 32, 36 and 40 min) between 400 nm–800 nm wavelength band. The percentage of degradation of dye was evaluated using the equation:

$$\%\text{Degradation} = \left(\frac{(C_0 - C_t)}{C_0}\right) \times 100, \quad (3)$$

C_0 is the initial concentration of dye (mg/mL) and C_t is the concentration of dye (mg/mL) at time t (min). The rate constant k was also computed where k = to understand

the kinetics of the photocatalytic degradation. The wavelength of the UV lamp is in the range 90–1100 nm, frequency is 50–60 Hz and power consumption was between 100–240 volts AC.

3.2.7. Anti-Inflammatory Activity of ZnO Nanoparticles

The anti-inflammatory activity was analyzed by COX assay using the method of Walker & Gierse, (2010) [98]. RAW 264.7 cells were grown to 60% confluency, followed by activation with 1 µL lipopolysaccharide (LPS) (1 µg/mL). LPS stimulated RAW cells were exposed to different concentrations (25 µg/mL, 50 µg/mL and 100 µg/mL) of Zn nanoparticles and standard drug Acetylsalicylic acid. The exposed cells were incubated for 24 h, lysated by centrifugation and supernatant taken for the experiment. 100 µL of cell supernatant was incubated in Tris-HCl buffer (pH 8), glutathione 5 mM/L, and haemoglobin 5 mM/L for 1 min at 25 °C. The reaction was initiated by adding 200 mM/L arachidonic acid and terminated after 20 min of incubation at 37 °C, by adding 200 µL of the solution containing 10% trichloroacetic acid in 1 N hydrochloric acid. After the centrifugal separation and the addition of 200 µL of a 1% thiobarbiturate, the tubes were boiled for 20 min. The tubes were cooled and centrifuged for 3 min. The optical density measured at 632 nm was used to determine COX inhibition. All the experiments were done in triplicate to concede the results.

Percentage inhibition of the enzyme was calculated as,

$$\% \text{ inhibition} = ((\text{Absorbance of control} - \text{Absorbance of test})/(\text{Absorbance of control})) \times 100 \quad (4)$$

3.2.8. Antimicrobial Activity of ZnO Nanoparticles

The antimicrobial activity of green synthesized ZnO nanoparticles from the extract of *Acacia caesia* (L.) *Willd.* was tested using the agar well diffusion method [99]. The human pathogenic microorganisms used in this study included two bacterial strains (*Escherichia coli* ATCC 25922 and *Staphylococcus aureus* ATCC 25923) and two fungal strains (*Aspergillus niger* ATCC 16404 and *Candida albicans* ATCC 10231). Petriplates containing 20 mL Muller Hinton Agar Medium were seeded with bacterial strains (growth of culture adjusted according to McFarland Standard, 0.5%). Potato Dextrose agar plates were prepared and overnight grown species of fungi were swabbed. Wells of approximately 10 mm was bored using a well cutter and different concentrations of ZnO nanoparticles such as 250 µg/mL, 500 µg/mL and 1000 µg/mL was added. The plates were then incubated at 37 °C for 24 h for bacteria and at 28 °C for 48 h for fungi. The antimicrobial activity was assayed by measuring the diameter of the inhibition zone formed around the well (NCCLS, 1993). Streptomycin (antibiotic) and Clotrimazole (antimycotic) were used as a positive control.

4. Conclusions

Zinc oxide nanoparticles were successfully fabricated using the green synthesis facilitated method using the bark extract of *Acacia caesia* (L.) *Willd.*. The study reports a non-toxic, inexpensive and environmentally friendly method of nanoparticle synthesis. The presence of nanoparticles was confirmed by SEM analysis and UVspectrum revealed the compound as Zinc oxide whose composition was provided by EDX spectrum. XRD spectrum identified the size and shape of the nanoparticle. The size of the nanoparticle crystals showed a distribution in the range 31.1 ± 5.4 nm. The functional group present in the synthesized nanoparticles was examined through FTIR spectroscopy. Photocatalytic activity showed a dye degradation of 92.2% within 40 min, which makes it a potential candidate for water treatment. Furthermore, the produced nanoparticles were used for the antibacterial, antifungal and inflammatory studies. Agar well diffusion method was used to evaluate the antimicrobial activity of the ZnO nanoparticles against human pathogenic bacteria *Escherichia coli* and *Staphylococcus aureus*. It showed significant antibacterial activity at all concentrations. The antifungal activity against *Aspergillus niger* and *Candida albicans* showed fungicidal property at high concentration of the ZnO nanoparticles. The anti-inflammatory activity was analyzed by COX assay using RAW 264.7 cells, which showed

high potential to reducing inflammation. These studies showed that ZnO nanoparticles might be a promising option for microbicide and antiinflammatory agent.

Author Contributions: Conceptualization, J.A.; Data curation, T.R.A. and A.B.R.; Formal analysis, J.A., T.R.A., A.B.R. and G.M.T.; Funding acquisition, A.S.N.; Investigation, J.A.; Methodology, J.A. and T.R.A.; Project administration, A.S.N.; Resources, A.B.R. and G.M.T.; Supervision, A.S.N.; Validation, T.R.A. and A.S.N.; Writing – original draft, J.A., T.R.A., A.B.R. and G.M.T.; Writing – review & editing, A.S.N. All authors have read and agreed to the published version of the manuscript.

Funding: This research received no external funding.

Data Availability Statement: Not applicable.

Acknowledgments: The authors would like to acknowledge Department of Computational Biology and Bioinformatics and State Inter-University Centre for Excellence in Bioinformatics (SIUCEB), for extending necessary facilities. The authors also acknowledge the Central Laboratory for instrumentation and facilitation (CLIF), the University of Kerala for their technical support in sample analysis.

Conflicts of Interest: All authors declare no conflict of interest.

References

1. Poole, C.P., Jr.; Owens, F.J. *Introduction to Nanotechnology*; John Wiley & Sons: Hoboken, NJ, USA, 2003.
2. Mazzola, L. Commercializing nanotechnology. *Nat. Biotechnol.* **2003**, *21*, 1137–1143. [CrossRef] [PubMed]
3. Bobo, D.; Robinson, K.J.; Islam, J.; Thurecht, K.J.; Corrie, S.R. Nanoparticle-based medicines: A review of FDA-approved materials and clinical trials to date. *Pharm. Res.* **2016**, *33*, 2373–2387. [CrossRef]
4. Chen, G.; Roy, I.; Yang, C.; Prasad, P.N. Nanochemistry and nanomedicine for nanoparticle-based diagnostics and therapy. *Chem. Rev.* **2016**, *116*, 2826–2885. [CrossRef]
5. Ahmed, S.; Ahmad, M.; Swami, B.L.; Ikram, S. A review on plants extract mediated synthesis of silver nanoparticles for antimicrobial applications: A green expertise. *J. Adv. Res.* **2016**, *7*, 17–28. [CrossRef] [PubMed]
6. Sirelkhatim, A.; Mahmud, S.; Seeni, A.; Kaus, N.H.M.; Ann, L.C.; Bakhori, S.K.M.; Hasan, H.; Mohamad, D. Review on zinc oxide nanoparticles: Antibacterial activity and toxicity mechanism. *Nano-Micro Lett.* **2015**, *7*, 219–242. [CrossRef] [PubMed]
7. Jianrong, C.; Yuqing, M.; Nongyue, H.; Xiaohua, W.; Sijiao, L. Nanotechnology and biosensors. *Biotechnol. Adv.* **2004**, *22*, 505–518. [CrossRef]
8. Holzinger, M.; Le Goff, A.; Cosnier, S. Nanomaterials for biosensing applications: A review. *Front. Chem.* **2014**, *2*, 63. [CrossRef]
9. Awwad, A.M.; Salem, N.M.; Abdeen, A.O. Nanotechnology. Biosynthesis of silver nanoparticles using Olea europaea leaves extract and its antibacterial activity. *Nanosci. Nanotechnol.* **2012**, *2*, 164–170. [CrossRef]
10. McNeil, S.E. Nanotechnology for the biologist. *J. Leukoc. Biol.* **2005**, *78*, 585–594. [CrossRef]
11. Vaseem, M.; Umar, A.; Hahn, Y.-B. ZnO nanoparticles: Growth, properties, and applications. *Met. Oxide Nanostruct. Appl.* **2010**, *5*, 1–36.
12. Meulenkamp, E.A. Synthesis and growth of ZnO nanoparticles. *J. Phys. Chem. B* **1998**, *102*, 5566–5572.
13. Wu, C.; Qiao, X.; Chen, J.; Wang, H.; Tan, F.; Li, S. A novel chemical route to prepare ZnO nanoparticles. *Mater. Lett.* **2006**, *60*, 1828–1832. [CrossRef]
14. Hudlikar, M.; Joglekar, S.; Dhaygude, M.; Kodam, K. Latex-mediated synthesis of ZnS nanoparticles: Green synthesis approach. *J. Nanopart. Res.* **2012**, *14*, 865. [CrossRef]
15. Madhumitha, G.; Elango, G.; Roopan, S.M. Biotechnological aspects of ZnO nanoparticles: Overview on synthesis and its applications. *Appl. Microbiol. Biotechnol.* **2016**, *100*, 571–581. [CrossRef]
16. Vidya, C.; Hiremath, S.; Chandraprabha, M.; Antonyraj, M.L.; Gopal, I.V.; Jain, A.; Bansal, K. Green synthesis of ZnO nanoparticles by Calotropis gigantea. *Int. J. Curr. Eng. Technol.* **2013**, *1*, 118–120.
17. Agarwal, H.; Kumar, S.V.; Rajeshkumar, S. A review on green synthesis of zinc oxide nanoparticles—An eco-friendly approach. *Resour.-Effic. Technol.* **2017**, *3*, 406–413. [CrossRef]
18. Bhuyan, T.; Mishra, K.; Khanuja, M.; Prasad, R.; Varma, A. Biosynthesis of zinc oxide nanoparticles from Azadirachta indica for antibacterial and photocatalytic applications. *Mater. Sci. Semicond. Process.* **2015**, *32*, 55–61. [CrossRef]
19. Mason, C.; Vivekanandhan, S.; Misra, M.; Mohanty, A.K. Engineering. Switchgrass (Panicum virgatum) extract mediated green synthesis of silver nanoparticles. *World J. Nano Sci. Eng.* **2012**, *2*, 47. [CrossRef]
20. Otari, S.; Patil, R.; Nadaf, N.; Ghosh, S.; Pawar, S. Green biosynthesis of silver nanoparticles from an actinobacteria *Rhodococcus* sp. *Mater. Lett.* **2012**, *72*, 92–94. [CrossRef]
21. Mashrai, A.; Khanam, H.; Aljawfi, R.N. Biological synthesis of ZnO nanoparticles using C. albicans and studying their catalytic performance in the synthesis of steroidal pyrazolines. *Arab. J. Chem.* **2017**, *10*, S1530–S1536.
22. Azizi, S.; Ahmad, M.B.; Namvar, F.; Mohamad, R. Green biosynthesis and characterization of zinc oxide nanoparticles using brown marine macroalga Sargassum muticum aqueous extract. *Mater. Lett.* **2014**, *116*, 275–277. [CrossRef]

23. Anbuvannan, M.; Ramesh, M.; Viruthagiri, G.; Shanmugam, N.; Kannadasan, N. Anisochilus carnosus leaf extract mediated synthesis of zinc oxide nanoparticles for antibacterial and photocatalytic activities. *Mater. Sci. Semicond. Process.* **2015**, *39*, 621–628. [CrossRef]
24. Madan, H.; Sharma, S.; Suresh, D.; Vidya, Y.; Nagabhushana, H.; Rajanaik, H.; Anantharaju, K.; Prashantha, S.; Maiya, P.S. Facile green fabrication of nanostructure ZnO plates, bullets, flower, prismatic tip, closed pine cone: Their antibacterial, antioxidant, photoluminescent and photocatalytic properties. *Spectrochim. Acta Part A Mol. Biomol. Spectrosc.* **2016**, *152*, 404–416. [CrossRef]
25. Kalpana, V.; Devi Rajeswari, V. A review on green synthesis, biomedical applications, and toxicity studies of ZnO NPs. *Bioinorg. Chem. Appl.* **2018**, *2018*, 1–12. [CrossRef]
26. Sorescu, A.-A.; Ion, R.-M.; Ioana, Ş.-B. Green synthesis of silver nanoparticles using plant extracts. In Proceedings of the The 4th International Virtual Conference on Advanced Scientific Results, Zilina, Slovakia, 6–10 June 2016.
27. Dobrucka, R.; Długaszewska, J. Biosynthesis and antibacterial activity of ZnO nanoparticles using Trifolium pratense flower extract. *Saudi J. Biol. Sci.* **2016**, *23*, 517–523. [CrossRef]
28. Jafarirad, S.; Mehrabi, M.; Divband, B.; Kosari-Nasab, M. Biofabrication of zinc oxide nanoparticles using fruit extract of Rosa canina and their toxic potential against bacteria: A mechanistic approach. *Mater. Sci. Eng. C* **2016**, *59*, 296–302. [CrossRef]
29. Vanathi, P.; Rajiv, P.; Narendhran, S.; Rajeshwari, S.; Rahman, P.K.; Venckatesh, R. Biosynthesis and characterization of phyto mediated zinc oxide nanoparticles: A green chemistry approach. *Mater. Lett.* **2014**, *134*, 13–15. [CrossRef]
30. Raj, L.; Jayalakshmy, E. Biosynthesis and characterization of zinc oxide nanoparticles using root extract of Zingiber officinale. *Orient. J. Chem* **2015**, *31*, 51–56. [CrossRef]
31. Joel, C.; Badhusha, M.S.M. Green synthesis of ZnO Nanoparticles using Phyllanthus embilica Stem extract and their Antibacterial activity. *Der Pharm. Lett.* **2016**, *8*, 6.
32. Chavali, M.S.; Nikolova, M.P. Metal oxide nanoparticles and their applications in nanotechnology. *SN Appl. Sci.* **2019**, *1*, 1–30. [CrossRef]
33. Tereshchenko, A.; Bechelany, M.; Viter, R.; Khranovskyy, V.; Smyntyna, V.; Starodub, N.; Yakimova, R. Optical biosensors based on ZnO nanostructures: Advantages and perspectives. A review. *Sens. Actuators B Chem.* **2016**, *229*, 664–677. [CrossRef]
34. Jiang, J.; Pi, J.; Cai, J. The advancing of zinc oxide nanoparticles for biomedical applications. *Bioinorg. Chem. Appl.* **2018**, *2018*, 1062562. [CrossRef] [PubMed]
35. Xiong, H.M. ZnO nanoparticles applied to bioimaging and drug delivery. *Adv. Mater.* **2013**, *25*, 5329–5335. [CrossRef]
36. Zhang, Z.-Y.; Xiong, H.-M. Photoluminescent ZnO nanoparticles and their biological applications. *Materials* **2015**, *8*, 3101–3127. [CrossRef]
37. Mishra, P.K.; Mishra, H.; Ekielski, A.; Talegaonkar, S.; Vaidya, B. Zinc oxide nanoparticles: A promising nanomaterial for biomedical applications. *Drug Discov. Today* **2017**, *22*, 1825–1834. [CrossRef]
38. Rosi, N.L.; Mirkin, C.A. Nanostructures in biodiagnostics. *Chem. Rev.* **2005**, *105*, 1547–1562. [CrossRef] [PubMed]
39. Jamdagni, P.; Khatri, P.; Rana, J.S. Green synthesis of zinc oxide nanoparticles using flower extract of Nyctanthes arbor-tristis and their antifungal activity. *J. King Saud Univ.-Sci.* **2018**, *30*, 168–175. [CrossRef]
40. Benelli, G.; Kadaikunnan, S.; Alharbi, N.S.; Govindarajan, M. Biophysical characterization of Acacia caesia-fabricated silver nanoparticles: Effectiveness on mosquito vectors of public health relevance and impact on non-target aquatic biocontrol agents. *Environ. Sci. Pollut. Res.* **2018**, *25*, 10228–10242.
41. Babu, R.; Gautham, M.T.; Aswathy, T.; Indu, S.; Nair, A. Pharmacognostic and antibacterial activity evaluation of Acacia caesia (L.) Willd. *J. Pharmacogn. Phytochem.* **2020**, *9*, 48–54.
42. Suriyamoorthy, S.; Subramaniam, K.; Durai, S.J.R.; Wahaab, F.; Chitraselvi, R.P.E. Evaluation of wound healing activity of Acacia caesia in rats. *Wound Med.* **2014**, *7*, 1–7. [CrossRef]
43. Thambiraj, J.; Paulsamy, S. In vitro antioxidant potential of methanol extract of the medicinal plant, Acacia caesia (L.) Willd. *Asian Pac. J. Trop. Biomed.* **2012**, *2*, S732–S736. [CrossRef]
44. Abomuti, M.A.; Danish, E.Y.; Firoz, A.; Hasan, N.; Malik, M.A. Green Synthesis of Zinc Oxide Nanoparticles Using Salvia officinalis Leaf Extract and Their Photocatalytic and Antifungal Activities. *Biology* **2021**, *10*, 1075. [CrossRef] [PubMed]
45. Fu, L.; Fu, Z. Plectranthus amboinicus leaf extract–assisted biosynthesis of ZnO nanoparticles and their photocatalytic activity. *Ceram. Int.* **2015**, *41*, 2492–2496. [CrossRef]
46. Sakthivel, S.; Neppolian, B.; Shankar, M.; Arabindoo, B.; Palanichamy, M.; Murugesan, V. Solar photocatalytic degradation of azo dye: Comparison of photocatalytic efficiency of ZnO and TiO2. *Sol. Energy Mater. Sol. Cells* **2003**, *77*, 65–82. [CrossRef]
47. Lu, J.; Ali, H.; Hurh, J.; Han, Y.; Batjikh, I.; Rupa, E.J.; Anandapadmanaban, G.; Park, J.K.; Yang, D.-C. The assessment of photocatalytic activity of zinc oxide nanoparticles from the roots of Codonopsis lanceolata synthesized by one-pot green synthesis method. *Optik* **2019**, *184*, 82–89. [CrossRef]
48. Chen, S.; Chen, W.; Buyanova, I. Dynamics of donor bound excitons in ZnO. *Appl. Phys. Lett.* **2013**, *102*, 121103. [CrossRef]
49. Teke, A.; Özgür, Ü.; Doğan, S.; Gu, X.; Morkoç, H.; Nemeth, B.; Nause, J.; Everitt, H.O. Excitonic fine structure and recombination dynamics in single-crystalline ZnO. *Phys. Rev. B* **2004**, *70*, 195207. [CrossRef]
50. Aminuzzaman, M.; Ying, L.P.; Goh, W.-S.; Watanabe, A. Green synthesis of zinc oxide nanoparticles using aqueous extract of Garcinia mangostana fruit pericarp and their photocatalytic activity. *Bull. Mater. Sci.* **2018**, *41*, 1–10. [CrossRef]

51. Rafique, M.; Tahir, R.; Gillani, S.; Tahir, M.B.; Shakil, M.; Iqbal, T.; Abdellahi, M. Plant-mediated green synthesis of zinc oxide nanoparticles from Syzygium Cumini for seed germination and wastewater purification. *Int. J. Environ. Anal. Chem.* **2020**, *100*, 1–16. [CrossRef]
52. Spoială, A.; Ilie, C.-I.; Trușcă, R.-D.; Oprea, O.-C.; Surdu, V.-A.; Vasile, B.Ș.; Ficai, A.; Ficai, D.; Andronescu, E.; Dițu, L.-M. Zinc Oxide Nanoparticles for Water Purification. *Materials* **2021**, *14*, 4747. [CrossRef]
53. Mustapha, S.; Ndamitso, M.; Abdulkareem, A.; Tijani, J.; Shuaib, D.; Ajala, A.; Mohammed, A. Application of TiO_2 and ZnO nanoparticles immobilized on clay in wastewater treatment: A review. *Appl. Water Sci.* **2020**, *10*, 1–36. [CrossRef]
54. Wang, H.; Zhou, P.; Wang, J.; Wang, Y.; Wei, J.; Zhan, H.; Guo, R.; Zhang, Y. Synthesis and Characterization of Rectorite/ZnO/TiO_2 Composites and Their Properties of Adsorption and Photocatalysis for the Removal of Methylene Blue Dye. *J. Wuhan Univ. Technol.-Mater. Sci. Ed.* **2018**, *33*, 729–735. [CrossRef]
55. Weldegebrieal, G.K. Synthesis method, antibacterial and photocatalytic activity of ZnO nanoparticles for azo dyes in wastewater treatment: A review. *Inorg. Chem. Commun.* **2020**, *120*, 108140. [CrossRef]
56. Behnajady, M.A.; Modirshahla, N.; Shokri, M.; Zeininezhad, A.; Zamani, H.A. Enhancement photocatalytic activity of ZnO nanoparticles by silver doping with optimization of photodeposition method parameters. *J. Environ. Sci. Health Part A* **2009**, *44*, 666–672. [CrossRef]
57. Ameen, F.; Dawoud, T.; AlNadhari, S. Ecofriendly and low-cost synthesis of ZnO nanoparticles from Acremonium potronii for the photocatalytic degradation of azo dyes. *Environ. Res.* **2021**, *202*, 111700. [CrossRef] [PubMed]
58. Manoharan, C.; Pavithra, G.; Dhanapandian, S.; Dhamodaran, P.; Shanthi, B. Properties of spray pyrolised ZnO: Sn thin films and their antibacterial activity. *Spectrochim. Acta Part A Mol. Biomol. Spectrosc.* **2015**, *141*, 292–299. [CrossRef] [PubMed]
59. Jiang, Y.; Zhang, L.; Wen, D.; Ding, Y. Role of physical and chemical interactions in the antibacterial behavior of ZnO nanoparticles against *E. coli*. *Mater. Sci. Eng. C* **2016**, *69*, 1361–1366. [CrossRef]
60. Miri, A.; Mahdinejad, N.; Ebrahimy, O.; Khatami, M.; Sarani, M. Zinc oxide nanoparticles: Biosynthesis, characterization, antifungal and cytotoxic activity. *Mater. Sci. Eng. C* **2019**, *104*, 109981. [CrossRef] [PubMed]
61. Gur, T.; Meydan, I.; Seckin, H.; Bekmezci, M.; Sen, F. Green synthesis, characterization and bioactivity of biogenic zinc oxide nanoparticles. *Environ. Res.* **2022**, *204*, 111897. [CrossRef] [PubMed]
62. Raghupathi, K.R.; Koodali, R.T.; Manna, A.C. Size-dependent bacterial growth inhibition and mechanism of antibacterial activity of zinc oxide nanoparticles. *Langmuir* **2011**, *27*, 4020–4028. [CrossRef]
63. Padmavathy, N.; Vijayaraghavan, R. Enhanced bioactivity of ZnO nanoparticles—An antimicrobial study. *Sci. Technol. Adv. Mater.* **2008**, *9*, 035004. [CrossRef] [PubMed]
64. Zhang, L.; Jiang, Y.; Ding, Y.; Povey, M.; York, D. Investigation into the antibacterial behaviour of suspensions of ZnO nanoparticles (ZnO nanofluids). *J. Nanopart. Res.* **2007**, *9*, 479–489. [CrossRef]
65. Ahmed, B.; Solanki, B.; Zaidi, A.; Khan, M.S.; Musarrat, J. Bacterial toxicity of biomimetic green zinc oxide nanoantibiotic: Insights into ZnONP uptake and nanocolloid–bacteria interface. *Toxicol. Res.* **2019**, *8*, 246–261. [CrossRef] [PubMed]
66. Murali, M.; Kalegowda, N.; Gowtham, H.G.; Ansari, M.A.; Alomary, M.N.; Alghamdi, S.; Shilpa, N.; Singh, S.B.; Thriveni, M.; Aiyaz, M. Plant-Mediated Zinc Oxide Nanoparticles: Advances in the New Millennium towards Understanding Their Therapeutic Role in Biomedical Applications. *Pharmaceutics* **2021**, *13*, 1662. [CrossRef] [PubMed]
67. Nagajyothi, P.; Cha, S.J.; Yang, I.J.; Sreekanth, T.; Kim, K.J.; Shin, H.M. Antioxidant and anti-inflammatory activities of zinc oxide nanoparticles synthesized using Polygala tenuifolia root extract. *J. Photochem. Photobiol. B Biol.* **2015**, *146*, 10–17. [CrossRef] [PubMed]
68. Jayachandran, A.; Aswathy, T.; Nair, A.S. Green synthesis and characterization of zinc oxide nanoparticles using Cayratia pedata leaf extract. *Biochem. Biophys. Rep.* **2021**, *26*, 100995. [CrossRef] [PubMed]
69. Talam, S.; Karumuri, S.R.; Gunnam, N. Synthesis, characterization, and spectroscopic properties of ZnO nanoparticles. *Int. Sch. Res. Not.* **2012**, *2012*, 372505. [CrossRef]
70. Fouda, A.; Salem, S.S.; Wassel, A.R.; Hamza, M.F.; Shaheen, T.I. Optimization of green biosynthesized visible light active CuO/ZnO nano-photocatalysts for the degradation of organic methylene blue dye. *Heliyon* **2020**, *6*, e04896. [CrossRef]
71. El-Belely, E.F.; Farag, M.; Said, H.A.; Amin, A.S.; Azab, E.; Gobouri, A.A.; Fouda, A. Green synthesis of zinc oxide nanoparticles (ZnO-NPs) using Arthrospira platensis (Class: Cyanophyceae) and evaluation of their biomedical activities. *Nanomaterials* **2021**, *11*, 95. [CrossRef] [PubMed]
72. Fakhari, S.; Jamzad, M.; Kabiri Fard, H. Green synthesis of zinc oxide nanoparticles: A comparison. *Green Chem. Lett. Rev.* **2019**, *12*, 19–24. [CrossRef]
73. Alberti, S.; Basciu, I.; Vocciante, M.; Ferretti, M. Experimental and Physico-Chemical Comparison of ZnO Nanoparticles' Activity for Photocatalytic Applications in Wastewater Treatment. *Catalysts* **2021**, *11*, 678. [CrossRef]
74. Ochieng, P.; Iwuoha, E.; Michira, I.; Masikini, M.; Ondiek, J.; Githira, P.; Kamau, G. Green route synthesis and characterization of ZnO nanoparticles using Spathodea campanulata. *Int. J. Biochem. Phys.* **2015**, *23*, 53–61.
75. Wang, J.; Wang, Z.; Huang, B.; Ma, Y.; Liu, Y.; Qin, X.; Zhang, X.; Dai, Y. Oxygen vacancy induced band-gap narrowing and enhanced visible light photocatalytic activity of ZnO. *ACS Appl. Mater. Interfaces* **2012**, *4*, 4024–4030. [CrossRef] [PubMed]
76. Muhammad, W.; Ullah, N.; Haroon, M.; Abbasi, B.H. Optical, morphological and biological analysis of zinc oxide nanoparticles (ZnO NPs) using *Papaver somniferum* L. *RSC Adv.* **2019**, *9*, 29541–29548. [CrossRef]

77. Frost, R.; Ding, Z.; Martens, W.; Johnson, T.; Kloprogge, J.T. Molecular assembly in synthesised hydrotalcites of formula CuxZn6—x$Al_2(OH)_{16}(CO_3)\cdot 4H_2O$—A vibrational spectroscopic study. *Spectrochim. Acta Part A Mol. Biomol. Spectrosc.* **2003**, *59*, 321–328. [CrossRef]
78. Chen, C.; Yu, B.; Liu, P.; Liu, J.; Wang, L. Investigation of nano-sized ZnO particles fabricated by various synthesis routes. *J. Ceram. Process. Res.* **2011**, *12*, 420–425.
79. Yu, P.; Yu, H.; Sun, Q.; Ma, B. Filter paper supported nZVI for continuous treatment of simulated dyeing wastewater. *Sci. Rep.* **2019**, *9*, 1–8.
80. Rambabu, K.; Bharath, G.; Banat, F.; Show, P.L. Green synthesis of zinc oxide nanoparticles using Phoenix dactylifera waste as bioreductant for effective dye degradation and antibacterial performance in wastewater treatment. *J. Hazard. Mater.* **2021**, *402*, 123560. [CrossRef] [PubMed]
81. Marin-Flores, C.A.; Rodríguez-Nava, O.C.; García-Hernández, M.; Ruiz-Guerrero, R.; Juárez-López, F.; de Jesús Morales-Ramírez, A. Free-radical scavenging activity properties of ZnO sub-micron particles: Size effect and kinetics. *J. Mater. Res. Technol.* **2021**, *13*, 1665–1675. [CrossRef]
82. Zare, M.; Namratha, K.; Alghamdi, S.; Mohammad, Y.H.E.; Hezam, A.; Zare, M.; Drmosh, Q.A.; Byrappa, K.; Chandrashekar, B.N.; Ramakrishna, S. Novel green biomimetic approach for synthesis of ZnO-Ag nanocomposite; antimicrobial activity against food-borne pathogen, biocompatibility and solar photocatalysis. *Sci. Rep.* **2019**, *9*, 1–15.
83. Surendra, B.; Mallikarjunaswamy, C.; Pramila, S.; Rekha, N. Bio-mediated synthesis of ZnO nanoparticles using Lantana Camara flower extract: Its characterizations, photocatalytic, electrochemical and anti-inflammatory applications. *Environ. Nanotechnol. Monit. Manag.* **2021**, *15*, 100442.
84. Ilves, M.; Palomäki, J.; Vippola, M.; Lehto, M.; Savolainen, K.; Savinko, T.; Alenius, H. Topically applied ZnO nanoparticles suppress allergen induced skin inflammation but induce vigorous IgE production in the atopic dermatitis mouse model. *Part. Fibre Toxicol.* **2014**, *11*, 1–12. [CrossRef]
85. Ramesh, P.; Saravanan, K.; Manogar, P.; Johnson, J.; Vinoth, E.; Mayakannan, M. Green synthesis and characterization of biocompatible zinc oxide nanoparticles and evaluation of its antibacterial potential. *Sens. Bio-Sens. Res.* **2021**, *31*, 100399. [CrossRef]
86. Getie, S.; Belay, A.; Chandra Reddy, A.; Belay, Z. Synthesis and characterizations of zinc oxide nanoparticles for antibacterial applications. *J. Nanomed. Nanotechno. S* **2017**, *8*, 1–8.
87. Sepasgozar, S.M.E.; Mohseni, S.; Feizyzadeh, B.; Morsali, A. Green synthesis of zinc oxide and copper oxide nanoparticles using Achillea Nobilis extract and evaluating their antioxidant and antibacterial properties. *Bull. Mater. Sci.* **2021**, *44*, 1–13. [CrossRef]
88. Agarwal, H.; Menon, S.; Kumar, S.V.; Rajeshkumar, S. Mechanistic study on antibacterial action of zinc oxide nanoparticles synthesized using green route. *Chemico-Biol. Interact.* **2018**, *286*, 60–70. [CrossRef]
89. Soren, S.; Kumar, S.; Mishra, S.; Jena, P.K.; Verma, S.K.; Parhi, P. Evaluation of antibacterial and antioxidant potential of the zinc oxide nanoparticles synthesized by aqueous and polyol method. *Microb. Pathog.* **2018**, *119*, 145–151. [CrossRef]
90. Jayaseelan, C.; Rahuman, A.A.; Kirthi, A.V.; Marimuthu, S.; Santhoshkumar, T.; Bagavan, A.; Gaurav, K.; Karthik, L.; Rao, K.B. Novel microbial route to synthesize ZnO nanoparticles using Aeromonas hydrophila and their activity against pathogenic bacteria and fungi. *Spectrochim. Acta Part A Mol. Biomol. Spectrosc.* **2012**, *90*, 78–84. [CrossRef]
91. Pillai, A.M.; Sivasankarapillai, V.S.; Rahdar, A.; Joseph, J.; Sadeghfar, F.; Rajesh, K.; Kyzas, G.Z. Green synthesis and characterization of zinc oxide nanoparticles with antibacterial and antifungal activity. *J. Mol. Struct.* **2020**, *1211*, 128107. [CrossRef]
92. Siddiqi, K.S.; ur Rahman, A.; Husen, A. Properties of zinc oxide nanoparticles and their activity against microbes. *Nanoscale Res. Lett.* **2018**, *13*, 1–13. [CrossRef]
93. da Silva, B.L.; Abuçafy, M.P.; Manaia, E.B.; Junior, J.A.O.; Chiari-Andréo, B.G.; Pietro, R.C.R.; Chiavacci, L.A. Relationship between structure and antimicrobial activity of zinc oxide nanoparticles: An overview. *Int. J. Nanomed.* **2019**, *14*, 9395. [CrossRef]
94. Tan, S.; Sun, X.; Zhang, X.; Chua, S.; Chen, B.; Teo, C. Cluster coarsening in zinc oxide thin films by postgrowth annealing. *J. Appl. Phys.* **2006**, *100*, 033502. [CrossRef]
95. Baharudin, K.B.; Abdullah, N.; Derawi, D. Effect of calcination temperature on the physicochemical properties of zinc oxide nanoparticles synthesized by coprecipitation. *Mater. Res. Express* **2018**, *5*, 125018. [CrossRef]
96. Ismail, A.; Menazea, A.; Kabary, H.A.; El-Sherbiny, A.; Samy, A. The influence of calcination temperature on structural and antimicrobial characteristics of zinc oxide nanoparticles synthesized by Sol–Gel method. *J. Mol. Struct.* **2019**, *1196*, 332–337. [CrossRef]
97. Viezbicke, B.D.; Patel, S.; Davis, B.E.; Birnie, D.P., III. Evaluation of the Tauc method for optical absorption edge determination: ZnO thin films as a model system. *Phys. Status Solidi B* **2015**, *252*, 1700–1710. [CrossRef]
98. Walker, M.C.; Gierse, J.K. In vitro assays for cyclooxygenase activity and inhibitor characterization. In *Cyclooxygenases*; Springer: Berlin/Heidelberg, Germany, 2010; pp. 131–144.
99. Álvarez-Chimal, R.; García-Pérez, V.I.; Álvarez-Pérez, M.A.; Arenas-Alatorre, J.Á. Green synthesis of ZnO nanoparticles using a Dysphania ambrosioides extract. Structural characterization and antibacterial properties. *Mater. Sci. Eng. C* **2021**, *118*, 111540. [CrossRef]